Journal of Crystal Growth 527 (2019) 125216

Contents lists available at ScienceDirect

Journal of Crystal Growth

journal homepage: www.elsevier.com/locate/jcrysgro

Strain stabilization of far from equilibrium GaAsBi films

Margaret A. Stevens, Kevin A. Grossklaus, Thomas E. Vandervelde*

Renewable Energy and Applied Photonics Labs, ECE Department, Tufts University, 161 College Avenue, Medford, MA 02155, USA

ARTICLE INFO

Communicated by H. Asahi

Keywords:
A3. molecular beam epitaxy
A1. segregation
B1. bismuth compounds
B2. semiconducting III-V materials

ABSTRACT

$GaAs_{1-x}Bi_x$ was grown on GaAs and InGaAs underlayers to determine the effect of global strain on bismuth (Bi) incorporation. Reducing compressive strain aids in Bi incorporation and results in higher Bi content films by preventing Ga-Bi surface droplet formation. A maximum Bi fraction of x = 0.088 was achieved in a 100 nm film on an $In_{0.105}GaAs$ buffer layer, a 24% relative improvement compared to layers grown on GaAs. Increasing Bi flux further did not result in incorporations past x = 0.088 on $In_{0.105}GaAs$ and strain could not be manipulated to incorporate more bismuth. Strain stabilization is thought to lessen Bi rejection and segregation, which increases the overall Bi content and yields homogenous films. The use of strain compensating layers can enable x = 0.06–0.09 content pseudomorphic $GaAs_{1-x}Bi_x$ films with uniform composition at thicknesses relevant for optoelectronic devices.

1. Introduction

Bismuth incorporation in GaAs ($GaAs_{1-x}Bi_x$) has resulted in III-V semiconductors that can span band gaps from GaAs to as low as 0.55 eV [1]. $GaAs_{1-x}Bi_x$ alloys grown on GaAs substrates open up new possibilities for solar cells [2–7], lasers [8–10], and LEDs [11]. Often, high bismuth incorporation in GaAsBi comes at the expense of surface quality as Ga-Bi droplets can form during growth [1,12]. These droplets result from the low V/III flux ratios that are critical for Bi incorporation in molecular beam epitaxy (MBE) growth [13,14]. While modeling the solubility of Bi in GaAs has shown gallium droplets aid in bismuth incorporation by providing an increased amount of gallium surface sites, Bi droplets have shown to be a Bi-sink on the growth surface of the alloy [15,16]. Although such droplets can be etched away after growth [1], their presence during the growth process can lead to unintended compositional variation through the thickness of the film [17]. The formation of these droplets, combined with the significant lattice mismatch between x > 0.07 GaAsBi and GaAs substrates, has limited the thickness of high Bi-content GaAsBi layers to < 50 nm [1,12] with the exception of authors who have found that using exceptionally high growth rates (> 1 μm/hr) can delay droplet formation for Bi fractions up to x = 0.12 [18].

Such progress in kinetically limited GaAsBi growth emphasizes the importance of droplet suppression for achieving higher Bi content in films of device relevant thicknesses. In this work, a method of droplet suppression through film strain manipulation is explored. Previous density functional theory calculations for Bi solubility in GaAs have shown a decrease in the formation energy of Bi in the crystal by applying in-plane global tensile strain [19]. Previous work on quaternary GaAsBi(N,P) alloys have shown a benefit to decreasing the local strain by replacing a fraction of the As in the crystal with a smaller atom such as nitrogen or phosphorus [20]. By growing quaternary alloys with balanced local strain, the authors increased bismuth incorporation beyond the initial bismuth saturation point, or the point where high Bi fluxes result in Bi droplet formation on the surface and further Bi incorporation is inhibited [15].

This work explores the impact of global strain on Bi solubility in GaAsBi. Relaxed InGaAs buffer layers were used to vary the in-plane compressive strain of GaAsBi capping layers. Reducing film strain allowed for more Bi to incorporate into the alloy, possibly by reducing anion exchange and lessening the energetic drive for phase separation. A relative increase in maximum Bi incorporation up to 24% was achieved for GaAsBi layers grown 100 nm thick on $In_{0.105}GaAs$ compared to when grown on GaAs. The excess bismuth that resulted in droplets on the surface of GaAsBi/GaAs films incorporates in the GaAsBi/$In_{0.105}GaAs$ alloy, resulting in nearly droplet-free films and no phase separation.

2. Experimental details

Samples were grown in a Veeco GENxplor MBE system with a valved As_4 cracker source and solid source effusion cells for Ga, In, and Bi. Quarter 2″ (0 0 1)-oriented epi-ready GaAs wafers were heated to 620 °C under As_4 overpressure to remove the native oxide. Temperature

* Corresponding author.
E-mail address: tvanderv@ece.tufts.edu (T.E. Vandervelde).

https://doi.org/10.1016/j.jcrysgro.2019.125216
Received 23 April 2019; Received in revised form 18 July 2019; Accepted 29 August 2019
Available online 30 August 2019

was monitored by band-edge thermometry (kSA BandiT) and surface reconstruction was monitored by reflection high energy electron diffraction (RHEED). 500 nm thick GaAs buffer layers were grown at 580 °C and at 1 ML/s. When used, 500 nm thick InGaAs buffer layers were grown at 480 °C and at 0.5–0.6 ML/s. After buffer growth, samples were cooled to 250 °C at 30 °C/min. GaAsBi layers were grown to 100 nm thick at 0.4–0.5 ML/s with an As_4/Ga beam equivalent pressure ratio (BEPR) of ~12.5 as measured by a retractable ion gauge. The Bi/Ga BEPR was tuned to achieve the desired Bi fraction.

Samples were characterized with high-resolution x-ray diffraction (HRXRD) on a Bruker D8 X-ray diffractometer to evaluate changes in lattice constant and film strain. 004 2θ/ω line scans were measured for each sample, and 224 reciprocal space maps (RSMs) were measured to confirm strain state and thus allow for more accurate determination of in and out of plane lattice parameter. GaAsBi fraction and strain were determined by HRXRD using Leptos simulations software, assuming a GaBi lattice constant of 0.633 nm, Vegard's law, and the elastic constants of GaAs [21]. No significant epilayer tilt was found in these measurements and the measurements of GaAsBi layer strain account for the partial relaxation of the InGaAs underlayer when necessary. Rutherford backscattering spectrometry (RBS) at 2.5 MeV was used to confirm measured Bi fraction for two samples grown on InGaAs buffer layers, as there was more uncertainty in the XRD simulation due to the partially relaxed InGaAs underlayer. Simulations using SIMNRA software [22] had a maximum deviation from the XRD results of x = 0.004. Therefore; XRD was chosen as the primary method of determining Bi fraction for the rest of the GaAsBi/InGaAs samples. Scanning transmission electron microscopy (STEM) on a JEOL 200F ARM at 200 kV was used to investigate phase separation with a high-angle annular dark field (HAADF) detector.

3. Results

To maximize Bi incorporation in $GaAs_{1-x}Bi_x$ films the Bi flux was increased while keeping the following experimental factors constant: As_4/Ga BEPR, group-III determined growth rate, and substrate temperature. The relationship between Bi fraction and Bi/Ga flux is linear for low Bi fractions, similar to what has been shown by previous authors [12,18,23,24]. For GaAsBi films grown on GaAs, the maximum Bi fraction achieved in this work was x = 0.071 at a Bi/Ga BEPR of 0.36. Fig. 1(a) shows the 004 2θ/ω HRXRD line scans used to determine Bi fraction for samples that were fully strained to the underlying GaAs, confirmed by 224 RSMs. For samples grown on GaAs, increasing the Bi/Ga BEPR from 0.36 (black curve) to 0.4 (gray curve) lead to a decrease in film peak intensity and a split of the film peak into three regions that increasingly shifted to higher 2θ, indicating smaller film lattice constants. The three distinct regions of the film peak are thought to be different regions of Bi content through the GaAsBi film. Samples grown in these flux conditions exhibit a (2 × 1) RHEED pattern that rapidly dimmed with growth, large Bi-Ga droplets on the surface and significant surface roughness between droplets. This RHEED behavior and resulting HRXRD results are indicative of Bi saturation in the film. Samples grown below the saturation point exhibited a (1 × 3) surface reconstruction and single film peaks.

If the linear relationship between Bi fraction and Bi/Ga BEPR had continued, the post-saturation sample would have resulted in a GaAsBi film with x = 0.082. Assuming a GaBi lattice constant of 0.633 nm, a Vegard's law relationship between GaAs and GaBi, and a GaAsBi Poisson's ratios matched to GaAs, a $GaAsBi_{0.082}$ film grown coherently strained to the GaAs substrate would have experienced an in-plane compressive strain of 0.97%. By growing on ~ 500 nm of partially relaxed $In_{0.105}GaAs$, the in-plane compressive strain is reduced to 0.50%. 004 2θ/ω HRXRD results from samples grown on $In_{0.105}GaAs$ buffer layers are shown in Fig. 1(b). The maximum relaxation of the $In_{0.105}GaAs$ buffer layers ranged from 63 to 74% as determined by 224 RSMs. Orthogonal 224 RSMs showed that the InGaAs layer experienced

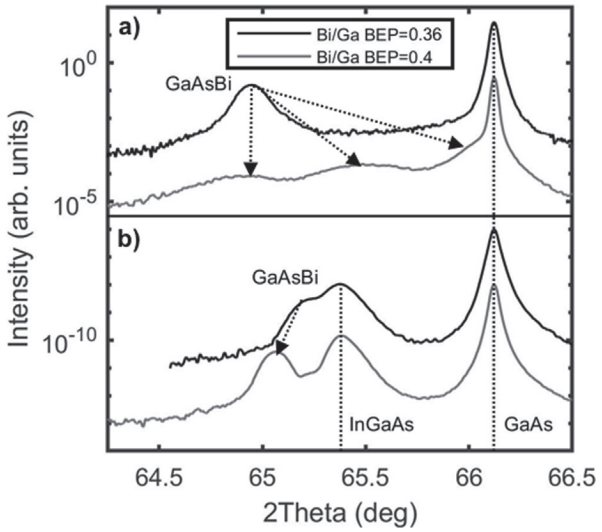

Fig. 1. HRXRD 004 2θ/ω line scans for GaAsBi films grown on both GaAs and $In_{0.105}GaAs$ buffer layers. The black lines indicate Bi/Ga = 0.36 BEPR while the gray lines indicate Bi/Ga = 0.4 BEPR. (a) Samples grown on GaAs with Bi/Ga = 0.4 appear to have poor film quality, phase separation, and decreased incorporation of Bi. (b) Samples grown on $In_{0.105}GaAs$ continue to incorporate Bi with a linear trend between Bi fraction and Bi/Ga BEPR.

asymmetric relaxation, where it is slightly more relaxed along the [1–10] crystallographic direction than it is along the [1 1 0] crystallographic direction (67% compared to 47%). This is interesting, in that the GaAsBi films grown coherently strained on top experiences an asymmetric in-plane strain, ranging from −0.49–0.61%. However, the incorporated Bi was found to be the same along both crystallographic directions in the XRD simulations. For samples grown on $In_{0.105}GaAs$, the GaAsBi film peak shifts to lower 2θ values with increasing Bi/Ga BEPR, indicating more Bi incorporated in the crystal. Fitting the 004 2θ/ω line scans and the 224 RSMs gives a Bi fraction of x = 0.084 for Bi/Ga = 0.4 BEPR grown on an $In_{0.105}GaAs$ buffer. In contrast to the case on GaAs buffer layers, increasing Bi flux results in higher incorporated Bi fraction.

AFM and optical microscopy, not shown, of the GaAsBi/InGaAs samples show reduced droplet formation alongside the increased Bi incorporation. Recent work on GaAsBi has shown that Ga-Bi droplet formation can cause vertical composition variations through the bulk film due to incorporation of gallium and bismuth into the droplets rather than into the lattice [17]. The bismuth-saturated GaAsBi films shown in this work have both vertical and lateral composition modulation found throughout the film. This occurs underneath the droplets that remain after samples were removed from the MBE chamber as well as underneath regions where droplets have migrated, leaving rough surfaces and tracks in their wake [13,14].

Fig. 2 shows HAADF STEM images for two samples with Bi/Ga = 0.4 and one sample with Bi/Ga = 0.5. In Fig. 2(a), the low-resolution STEM image shows a 2.5 μm wide viewing region near a Bi droplet, confirmed by EDS, not shown. Changes in the STEM contrast are indicative of changes in Bi content, where bright regions correspond to higher Bi content in these images. In Fig. 2(a), there is a region of higher Bi content near the GaAsBi/GaAs interface, a region of low Bi content directly above it, and capped with a region of higher Bi content in the last ~20 nm of the epilayer. The top region of higher Bi content is significantly thinner directly underneath the droplet, indicating that the evolution of the phase separation is related to Bi adatoms incorporating into the droplet rather than into the film as previously modeled [15]. In Fig. 2(b), the HAADF STEM image for the sample grown on $In_{0.105}GaAs$ shows uniform contrast through both the bulk of the film and the width of the viewing window. The uniform bismuth

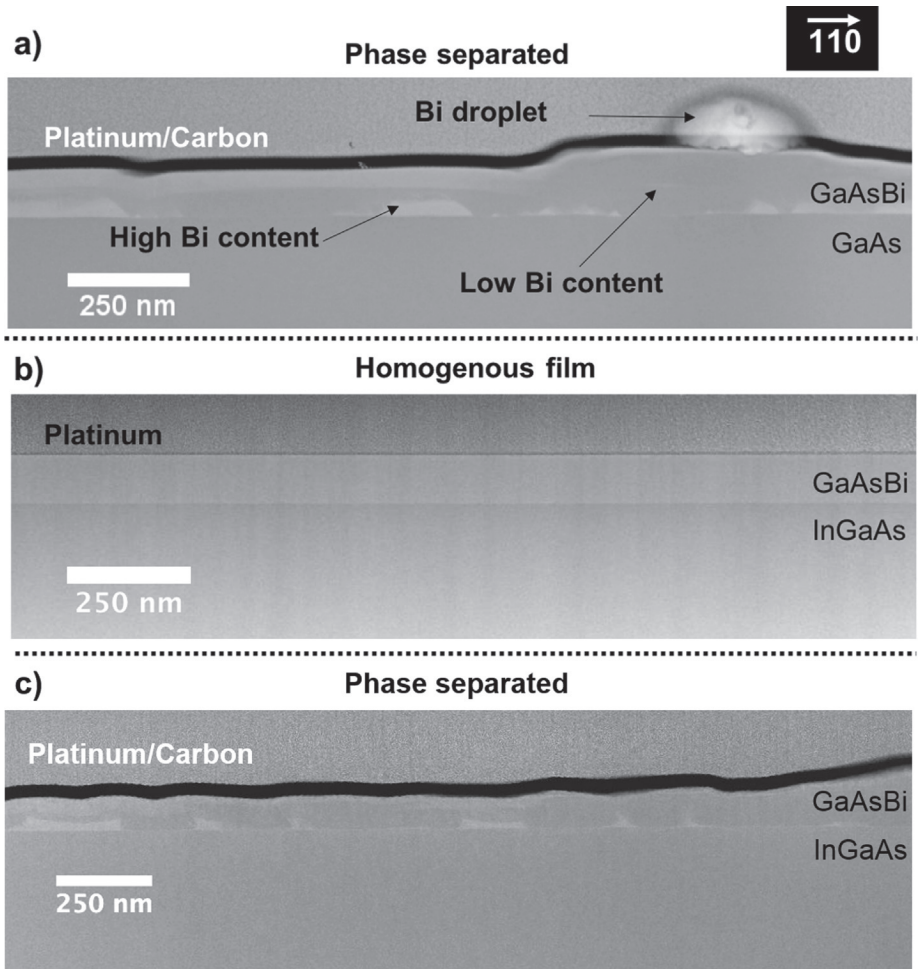

Fig. 2. (a) HAADF STEM image of GaAsBi/GaAs grown with Bi/Ga = 0.4 showing a Bi droplet on the surface as well as vertical phase separation in the bulk that varies along the GaAsBi/GaAs interface. (b) HAADF STEM image GaAsBi/InGaAs also grown with Bi/Ga = 0.4 but with reduced compressive strain on the epilayer. The film is uniform both laterally and vertically. (c) HAADF STEM image of phase separated GaAsBi/InGaAs/GaAs sample grown with Bi/Ga = 0.5.

incorporation throughout the film is attributed to the lack of surface droplets present when grown with reduced compressive strain.

As the Bi/Ga BEPR is further increased for samples grown on $In_{0.105}GaAs$, there is a point after Bi/Ga = 0.43 BEPR, resulting in x = 0.088, where large droplets form and further inhibit Bi from incorporating in the crystal. For Bi/Ga = 0.5 BEPR, the previous trend between Bi/Ga BEPR and Bi fraction would predict the epilayer to be $GaAsBi_{0.103}$. However, the film that grew under these conditions had negligible Bi incorporation according to HRXRD and significant droplet coverage on the surface (not shown), indicating droplet induced phase separation. The HAADF STEM image shown in Fig. 2(c) confirms this is the case, as the 100 nm film grown on $In_{0.105}GaAs$ has the similar platelet-like structure seen in Bi saturated sample shown in Fig. 2(a).

Fig. 3 shows the 224 RSMs for (a) Bi/Ga = 0.4 BEPR grown on $In_{0.105}GaAs$ and (b) Bi/Ga = 0.5 BEPR grown on $In_{0.105}GaAs$ underlayers. The InGaAs underlayers relaxed to 66% and 69%, respectively along the [1–10] direction. For Bi/Ga = 0.4 BEPR, shown in Fig. 3(a), the 100 nm GaAsBi film is fully compressively strained to the underlying $In_{0.105}GaAs$ layer. TEM imaging did not reveal any crystalline defects due to strain relaxation. In contrast, for Bi/Ga = 0.5 BEPR shown in Fig. 3(b), the 224 RSM shows a film tensile-strained to the $In_{0.105}GaAs$ buffer with some degree of strain relaxation as well as negligible Bi incorporation. TEM imaging, not shown, revealed some crystalline defects due to strain relaxation, as well as regions of compositional variation and regions characteristic of $CuPt_B$ atomic ordering along {1 1 1} planes. $CuPt_B$-type atomic ordering has previously been shown in the literature for GaAsBi [25,26] and GaAsBiN [27], and is thought to be linked to growth with the (2 × 1) surface reconstruction. While the actual film had negligible Bi incorporation, if the $GaAsBi_{0.103}$ film could have been stabilized, it would have resulted in an in-plane compressive strain of 0.70% along [1–10]. This strain could be reduced by growing on higher indium content InGaAs buffer layers.

However, further decreasing the expected in-plane compressive strain of the GaAsBi epilayer with Bi/Ga = 0.5 BEPR from 0.70% to 0.37% ($In_{0.15}GaAs$) to 0.23% ($In_{0.17}GaAs$), did not yield stable $GaAsBi_{0.10}$ layers at a thickness of 100 nm. All samples demonstrated RSMs akin to what is shown in Fig. 3(b), as well as a high density of Ga-Bi droplets on the surface. For both samples that saturate on GaAs and saturate on InGaAs buffers, the XRD results indicate that the film peak moves back towards GaAs lattice parameter, a sign of Bi rejection in the film. For samples that saturate on GaAs, this is expected, as rejecting the incoming bismuth reduces the strain on the material. However, for samples that saturate on InGaAs, rejecting the incoming bismuth moves the film into an unfavorable strain state, where the $GaAsBi_{<0.01}$ film is now tensile strained to the InGaAs underlayer. This behavior is indicative of a high energetic cost to achieving high Bi content in a 100 nm film, perhaps a greater cost than to form strain-related defects and relax. This also demonstrates an upper limit to the benefit of growing with reduced compressive strain for samples with x > 0.088, at least at film thicknesses of 100 nm or greater.

The overall trend shown in this work is displayed in Fig. 4(a). Samples grown on GaAs have clear Pendellösung fringes; therefore,

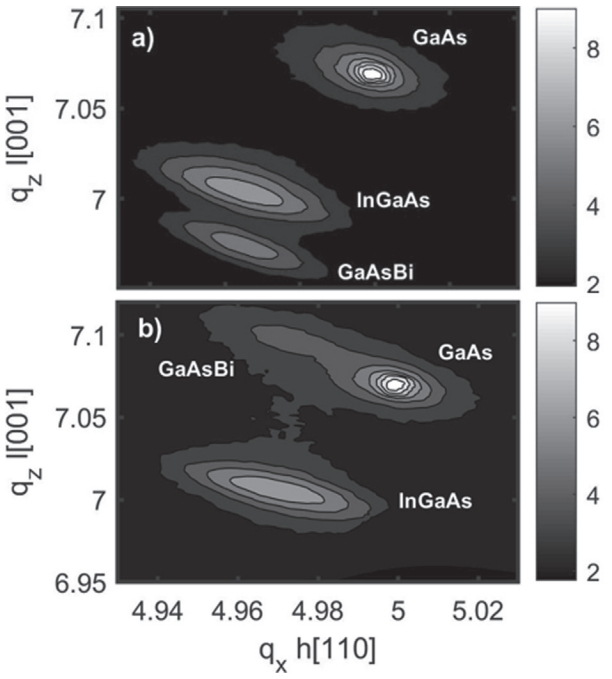

Fig. 3. 224 reciprocal space maps, plotted in q_x h[1 1 0] and q_z l[0 0 1] coordinates and on a log le for intensity, arbitrary units. (a) For Bi/Ga = 0.4 BEPR grown on $In_{0.105}GaAs$, the InGaAs film is 66% relaxed. The $GaAsBi_{0.084}$ film shows no signs of relaxation. (b) For Bi/Ga = 0.5 BEPR grown on $In_{0.105}GaAs$, the InGaAs film is 69% relaxed. The $GaAsBi_{< 0.01}$ film is tensile-strained to the underlying InGaAs layer and has begun to relax.

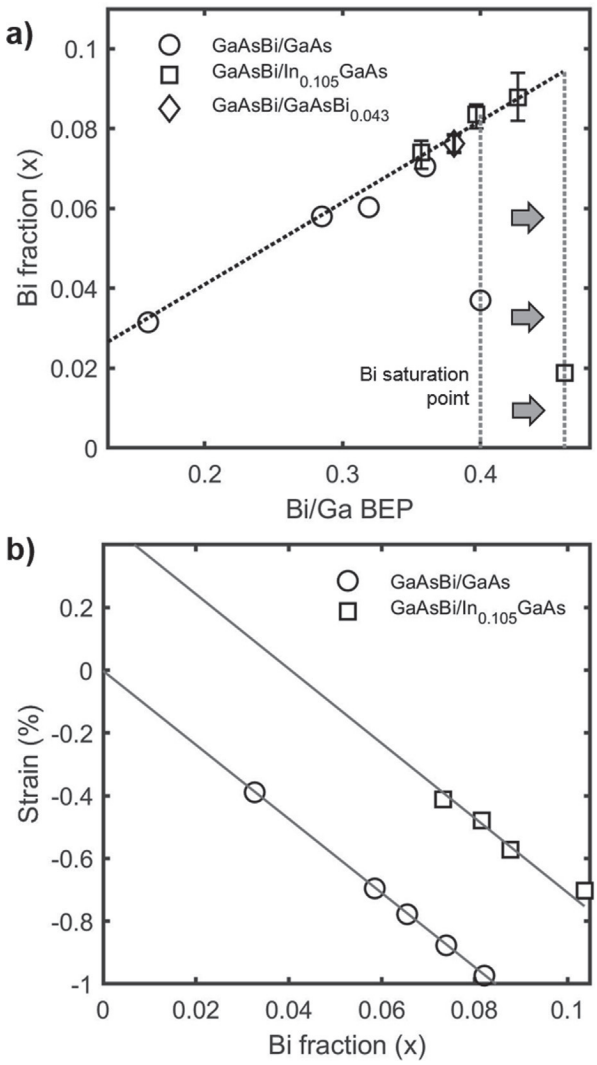

Fig. 4. (a) Bi fraction measured by XRD plotted against the Bi/Ga BEPR for samples grown on GaAs buffer layers (circles), $In_{0.105}GaAs$ buffer layers (squares), and a $GaAsBi_{0.043}$ buffer layer (diamond). (b) Epilayer strain as a function of the expected Bi fraction (x) in GaAsBi using the same symbol notation for the underlayers used. The gray lines represent the calculated epilayer strain assuming Vegard's law, 0.5653 nm for the GaAs lattice constant, and 0.568 nm for the InGaAs lattice constant.

there is negligible uncertainty in the XRD simulation. The samples grown on InGaAs and GaAsBi buffer layers demonstrate no Pendellösung fringes due to the relaxation of the buffer layer. For these samples, the error is determined by changing the buffer layer composition by 5% and recalculating the measured Bi fraction. Fig. 4(b) shows the calculated epilayer strain as a function of Bi fraction for films grown on GaAs substrates on and $In_{0.105}GaAs$ buffer layers. The symbols represent experimental data, using the expected Bi fraction from the Bi/Ga BEPR trend and the measured in-plane lattice constant of the underlayer. The lines represent the overall trend for strain as a function of Bi fraction, assuming Vegard's law, 0.5653 nm for the GaAs lattice constant, and 0.568 nm for the $In_{0.105}GaAs$ lattice constant. This can be used as a guide for understanding the strain conditions of the samples shown in Fig. 4(a). Bi fraction measured by HRXRD has a linear relationship to the Bi/Ga BEPR until large Ga-Bi droplets form. For samples grown on GaAs buffer layers (circles) the Bi fraction increases linearly up until x = 0.071 at Bi/Ga BEPR = 0.36. Samples with large Ga-Bi droplet formation, hindering Bi incorporation, are noted by the first vertical dashed line at Bi/Ga BEPR = 0.4. Decreasing the compressive strain by growing on ~500 nm of partially relaxed $In_{0.105}GaAs$ (squares) resulted in a shift in the Bi saturation point and continued linear incorporation of Bi. Samples on InGaAs with large Ga-Bi droplets and decreased Bi fraction are noted with a dashed line at Bi/Ga BEPR = 0.5. With this technique, the highest Bi incorporation achieved for GaAsBi/$In_{0.105}GaAs$/GaAs is x = 0.088 using Bi/Ga BEPR = 0.43, resulting in an in-plane compressive strain of 0.603%. This is a 24% relative increase in Bi incorporation compared to what was achieved in this work for GaAsBi/GaAs.

To decouple the effects of strain from underlayer surface composition or surface reconstruction, higher Bi content GaAsBi epilayers were grown on a 500 nm partially relaxed $GaAsBi_{0.043}$ buffer layer (diamond icon). Samples grown on $In_{0.105}GaAs$ buffer layers exhibited at (4 × 3) RHEED surface reconstruction before the start of GaAsBi growth. Samples grown on $GaAsBi_{0.043}$ exhibited a (1 × 3) RHEED surface reconstruction before the start of higher Bi fraction GaAsBi growth. Use of the $GaAsBi_{0.043}$ buffer layer changes the in-plane compressive strain to 0.51% for a top layer of $GaAsBi_{0.076}$. For a Bi/Ga BEPR = 0.38, this continues the linear trend between Bi fraction and the Bi/Ga BEPR.

Although much higher bismuth fractions (x > 0.10) have been achieved in the literature, most samples are < 50 nm thick [1,12] with the exception of samples grown under kinetically limited conditions, where GaAsBi with x = 0.10 has been grown to > 1 μm [18,25]. Kinetically limited bismide growth is typically achieved with fast growth rates (> 1 μm/hr). This aids in Bi incorporation by maintaining enough Bi on the surface to behave like a surfactant, but not so much that the incoming Bi adatoms form Bi droplets rather than incorporate. The role of this Bi surfactant layer (θ_{Bi}) has been found to be critical for achieving high Bi fractions while maintaining through-film uniformity [28,29].

Fig. 5 shows a schematic of the GaAsBi growth process, highlighting bismuth incorporation and rejection mechanisms that occur during the growth. Certain processes are heavily influenced by the bismuth flux such as (1) Bi absorption in θ_{Bi}. Other processes are more temperature

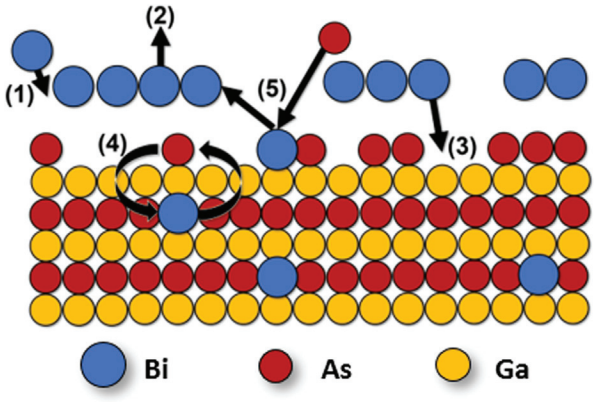

Fig. 5. Schematic of GaAsBi growth highlighting various Bi incorporation and rejection mechanisms: (1) absorption of Bi into θ_{Bi}, (2) desorption of Bi from θ_{Bi}, (3) Bi incorporation from θ_{Bi} into crystal (4) anion exchange with As, (5) removal of Bi from the crystal from incoming As.

dependent; such as (2) Bi desorption from θ_{Bi} and (3) Bi incorporation from θ_{Bi} into the film. Finally, other processes are highly dependent on the group-V flux such as (4) anion exchange in the first few monolayers of growth and (5) Bi removal from the growth surface by an As atom.

Many growth models have developed rate equations to describe these processes and as a result guide growth temperatures and flux ratios to maximize Bi incorporation [12,16,23]. These models do not account for the influence of strain that would explain the trends seen in this work. By reducing compressive strain, it is possible that the energetic barrier for Bi incorporation is reduced, similar to what has been shown for previous density functional theory studies [19]. Alternatively, while the Bi incorporation process (3) in Fig. 4(b) is thought to be determined by θ_{Bi}, the anion exchange process (4) as well as other Bi rejection mechanisms could be influenced by strain. By decreasing the compressive strain, it is possible that the higher Bi fraction alloy is more energetically stable and, therefore, less Bi rejection and phase separation occurs. It is possible that for large bismuth fractions ($x > 0.088$) the energetic cost of incorporating more bismuth is too high, and the change in the strain energy by reducing the compressive strain is not enough to compensate. In this case, the bismuth is rejected regardless of the underlayer choice and strain state of the film.

4. Conclusions

In this work, increased Bi incorporation in GaAsBi was achieved by growing with reduced in-plane compressive strain. By growing on relaxed buffer layers of $In_{0.105}GaAs$, the global strain of the epilayer was reduced and more Bi incorporated in the alloy instead of surface segregating and forming Ga-Bi droplets. Avoiding surface droplets improves film homogeneity by avoiding vertical and lateral compositional variation caused by surface droplets. These improvements were seen for a film thickness of 100 nm and compositions up to $GaAsBi_{0.088}$. For higher Bi fractions, the energetic benefit of reduced strain on the addition of Bi is insufficient to allow for more Bi incorporation, and droplets form regardless of the in-plane strain. With careful tuning of growth parameters, this technique can be used to grow higher-Bi content pseudomorphic films with uniform composition at optoelectronic device relevant thicknesses.

Acknowledgements

This work is supported by the Office of Naval Research (N00014-15-1-2946) and the NASA Space Technology Research Fellowship (NNX15AQ79H). Samples were grown in the Tufts Epitaxial Core Facility on equipment supported by the National Science Foundation (ECCS 1337783). Microscopy was performed at the Center for Nanoscale Systems (CNS) at Harvard University, supported by the National Science Foundation (NSF 1541959). X-ray diffraction was performed in the Shared Experimental Facilities at the Massachusetts Institute of Technology, supported in part by the MRSEC Program of the National Science Foundation (DMR 1419807). Rutherford backscattering spectrometry was performed at the Cambridge Laboratory for Accelerator-based Surface Science at the Massachusetts Institute of Technology.

References

[1] M. Masnadi-Shirazi, R.B. Lewis, V. Bahrami-Yekta, T. Tiedje, M. Chicoine, P. Servati, J. Appl. Phys. 116 (2014) 223506.
[2] T. Thomas, A. Mellor, N.P. Hylton, M. Fuhrer, D. Alonso-Alvarez, A. Braun, N.J. Ekins-Daukes, J.P.R. David, S.J. Sweeney, Semicond. Sci. Technol. 30 (2015) 094010.
[3] R.D. Richards, A. Mellor, F. Harun, J.S. Cheong, N.P. Hylton, T. Wilson, T. Thomas, J.S. Roberts, N.J. Ekins-Daukes, J.P.R. David, Sol. Energy Mater. Sol. Cells 172 (2017) 238.
[4] H. Kim, K. Kim, Y. Guan, J. Lee, T.F. Kuech, L.J. Mawst, Appl. Phys. Lett. 112 (2018) 251105.
[5] A. Zayan, M. Stevens, and T.E. Vandervelde, in 43rd IEEE Photovoltaics Spec. Conf. Proc. (2016), pp. 2839–2843.
[6] M. Stevens, A. Licht, N. Pfiester, E. Carlson, K. Grossklaus, and T. Vandervelde, in 44th IEEE Photovoltaics Spec. Conf. Proc. (2017), pp. 0701–0705.
[7] S.L. Lenney, K. Grossklaus, M. Stevens, T. Vandervelde, Terahertz, RF, Millimeter, Submilli.-Wave Technol. Appl. XII 109172A (2019).
[8] P. Ludewig, N. Knaub, N. Hossain, S. Reinhard, L. Nattermann, I.P. Marko, S.R. Jin, K. Hild, S. Chatterjee, S.J. Sweeney, K. Volz, Appl. Phys. Lett. 102 (2013) 2013.
[9] I.P. Marko, C.A. Broderick, S. Jin, P. Ludewig, W. Stolz, K. Volz, J.M. Rorison, E.P. O'Reilly, S.J. Sweeney, Sci. Rep. 6 (2016) 28863.
[10] X. Wu, W. Pan, Z. Zhang, Y. Li, C. Cao, J. Liu, L. Zhang, Y. Song, H. Ou, S. Wang, ACS Photon. 4 (2017) 1322.
[11] P.K. Patil, E. Luna, T. Matsuda, K. Yamada, K. Kamiya, F. Ishikawa, S. Shimomura, Nanotechnology 28 (2017) 105702.
[12] R.B. Lewis, M. Masnadi-Shirazi, T. Tiedje, Appl. Phys. Lett. 101 (2012) 082112.
[13] G. Vardar, S.W. Paleg, M.V. Warren, M. Kang, S. Jeon, R.S. Goldman, Appl. Phys. Lett. 102 (2013) 042106.
[14] E. Sterzer, N. Knaub, P. Ludewig, R. Straubinger, A. Beyer, K. Volz, J. Cryst. Growth 408 (2014) 71.
[15] G.V. Rodriguez, J.M. Millunchick, J. Appl. Phys. 120 (2016) 125310.
[16] C.R. Tait, J.M. Millunchick, J. Appl. Phys. 119 (2016) 215302.
[17] C.R. Tait, L. Yan, J.M. Millunchick, Appl. Phys. Lett. 111 (2017) 042105.
[18] A.J. Ptak, R. France, D.A. Beaton, K. Alberi, J. Simon, A. Mascarenhas, C.S. Jiang, J. Cryst. Growth 338 (2012) 107.
[19] H. Jacobsen, B. Puchala, T.F. Kuech, D. Morgan, Phys. Rev. B 86 (2012) 085207.
[20] L. Nattermann, P. Ludewig, E. Sterzer, K. Volz, J. Cryst. Growth 470 (2017) 15.
[21] S. Tixier, M. Adamcyk, T. Tiedje, S. Francoeur, A. Mascarenhas, P. Wei, F. Schiettekatte, Appl. Phys. Lett. 82 (2003) 2245.
[22] M. Mayer, in AIP Conf. Proc. (AIP, 1999), pp. 541–544.
[23] X. Lu, D.A. Beaton, R.B. Lewis, T. Tiedje, M.B. Whitwick, Appl. Phys. Lett. 92 (2008) 192110.
[24] M. Stevens, K. Grossklaus, J. McElearney, T.E. Vanderverde, J. Electron. Mater. 48 (2019) 3376.
[25] A.G. Norman, R. France, A.J. Ptak, J. Vac. Sci. Technol. B 29 (2011) 03C121.
[26] D.F. Reyes, F. Bastiman, C.J. Hunter, D.L. Sales, A.M. Sanchez, J.P.R. David, D. González, Nanoscale Res. Lett. 9 (2014) 23.
[27] J. Occena, T. Jen, H. Lu, B.A. Carter, T.S. Jimson, A.G. Norman, and R.S. Goldman, 113, 211602 (2018).
[28] F. Bastiman, A.G. Cullis, J.P.R. David, S.J. Sweeney, J. Cryst. Growth 341 (2012) 19.
[29] R.D. Richards, F. Bastiman, C.J. Hunter, D.F. Mendes, A.R. Mohmad, J.S. Roberts, J.P.R. David, J. Cryst. Growth 390 (2014) 120.